### = ATOMS, MOLECULES, OPTICS =

## METHODS AND SYSTEMS FOR COMPARING FREQUENCIES OF GEOGRAPHICALLY DISTANT OPTICAL STANDARDS

© 2024 A. V. Semenko\*, A. A. Karaush, D. M. Fedorova, A. N. Malimon, D. V. Sutyrin, S. N. Slyusarev, V. N. Fedotov and S. I. Donchenko

Federal State Unitary Enterprise "All-Russian Research Institute of Physical-Technical and Radio Engineering Measurements" (FSUE "VNIIFTRI"), Mendeleevo, Moscow Region, 141570 Russia

\*e-mail: av semenko@mail.ru

Received March 12, 2024 Kevised March 12, 2024 Accepted April 08, 2024

**Abstract**. Works for the future redefinition of the second based on quantum transition in the optical range are considered. The uncertainty budget of the Sr-1 optical frequency standard based on ultracold strontium atoms included in the State Primary Standard of Time and Frequency, is refined. Various methods for comparing frequencies of remote optical frequency standards are described to implement the "roadmap" adopted at the 27th General Conference on Weights and Measures. The accuracy characteristics maximally achievable when using the described methods are listed, and their comparison is given.

The article is presented as part of the conference proceedings "Physics of Ultracold Atoms" (PUCA-2023), Novosibirsk, December 2023.

#### **DOI:** 10.31857/S004445102410e043

#### 1. INTRODUCTION

Frequency standards are essential tools for defining the unit of time, the second. Currently, the valid definition of the second in the SI system is based on the microwave hyperfine transition in cesium atoms <sup>133</sup>Cs [1]. The cesium fountain and ensemble of hydrogen masers – time and frequency keepers, which are part of GET-1 - the State Primary Standard of Time and Frequency (SPSTF), participate in forming national and international time scales. Atomic clocks based on cesium fountains have reached the level of uncertainty in reproducing the frequency unit  $2.3 \cdot 10^{-16}$  [2]. and there are limitations that prevent significant improvement in their accuracy characteristics. Currently, optical frequency standards (OFS), that use optical transitions in atoms or ions as references have outperformed the best microwave standards in terms of stability and uncertainty of frequency reproduction. The main advantage of OFS over microwave standards is the higher frequency of "clock" transitions and narrower width of their spectral line.

The promising potential of OFS has been confirmed by research results from metrological institutes, including Russian ones. The best OFS have achieved frequency reproduction uncertainty at the level of  $1 \cdot 10^{-18}$  [3], and there are opportunities for further improvement of this indicator. This explains the aspiration of the metrological community, which is represented primarily by national metrology institutes, to adopt a new definition of the second based on an optical transition. According to the resolution adopted in 2022 at the 27th General Conference on Weights and Measures, by 2030 a new definition of the second based on a reference quantum transition in the optical range should be given [4].

Modern OFSs (Optical Frequency Standards) possess high accuracy characteristics, but their practical application is often hindered by their short continuous operation time (from several hours to several days), the complexity of comparing frequencies of laboratory OFSs located far from each other due to transportation impossibility and peculiarities of their radiation propagation

in communication channels. The Consultative Committee for Time and Frequency (CCTF) has recommended a "roadmap", viz. a series of practical steps necessary for redefining the second [4]. According to the roadmap, it is necessary both to clarify and improve the instability and uncertainty characteristics of existing OFSs and to ensure the possibility of high-precision frequency comparison of geographically distant OFSs, including on continental and intercontinental scales. Research aimed at improving the characteristics of existing OFSs and creating more accurate methods for comparing frequencies between geographically distant OFSs is relevant for implementing the new definition of the second. They will also be necessary for forming improved, i.e., more accurate, TAI (International Atomic Time, abbreviated TAI, from its French name "temps atomique international") and UTC (Universal Time Coordinated) scales. Remote frequency comparisons can be implemented by improving methods of transmitting highly stable optical radiation through compensated fiber-optic lines, using transportable OFSs, and developing comparison methods using Global Navigation Satellite System (GNSS) signals.

The comparison of standards is primarily necessary for forming the TAI scale based on the SI second and the UTC time scale. Note that the TAI time scale and UTC scale are formed by the International Bureau of Weights and Measures (BIPM) based on data about atomic clocks and their mutual comparisons received from cooperating national metrology laboratories. Currently, about ten primary frequency standards based on cesium atom fountains are operating worldwide. Only six laboratories, including All-Russian Scientific Research Institute for Physical-Engineering and Radiotechnical Metrology (VNIIFTRI), regularly provide their measurement results to BIPM, based on which BIPM establishes and maintains the TAI time scale [5].

VNIIFTRI has developed an optical frequency standard (OFS) based on ultracold strontium atoms (OFS Sr-1), included in GET-1 since 2018. Its residual systematic error (RSE) is not worse than  $1 \cdot 10^{-16}$ . In 2022, OFS Sr-2 and Sr-3 with improved RSE up to  $1 \cdot 10^{-17}$  due to reduced blackbody radiation were incorporated into GET-1. Currently, OFS Sr-1 is used to implement the national time scale in the test mode [6]. Development of a transportable

OFS (TOFS) based on ultracold Yb atoms [7] is also underway, along with research into reducing the mass and dimensional characteristics of such a standard [8].

In this work, we refine the most significant components of the uncertainty budget for OFS Sr-1, which is part of GET-1. We also briefly present a preliminary design for a transportable OFS using ultracold neutral atoms and discusses methods for comparing OFS frequencies with other geographically distant frequency standards.

### 2. REFINEMENT OF THE UNCERTAINTY BUDGET FOR OFS SR-1 INCLUDED IN GET-1

The OFS uncertainty budget is formed by several effects that make significant contributions to the RSE of the frequency shift relative to the unperturbed quantum transition. The greatest influence on the frequency of OFS using neutral Sr and Yb atoms comes from blackbody radiation, radiation from the optical lattice-forming laser (OLFL), and the Zeeman effect caused by magnetic field influence. There are other shifts whose effects on the OFS frequency are significantly smaller. These shifts include, for example, the shift dependent on atom density in the optical lattice, dynamic Stark shift, second-order Doppler shift, etc. The correction associated with them is at the level of units of  $10^{-17} - 10^{-18}$  digit. At the same time, the specified uncertainty value for the strontium atom OFS is determined at the level of  $1 \cdot 10^{-16}$ , and the first three indicated shifts contribute the most to it. For this reason, their RSE must be evaluated first. Below, we give the evaluation method and results.

## 2.1. Evaluation of the BBR shift contribution to RSE

The main sources of thermal radiation in optical frequency standards based on ultracold atoms Sr-1 are magnetic coils carrying electric current, the magnetic section of the Zeeman slower, thermal radiation in the infrared range passing through the vacuum chamber windows, and the source of hot strontium atoms, which is a furnace heated to temperature of 450°C with a 5 mm diameter hole located at a distance of 700 mm from the atoms.

The influence of various thermal radiation sources depends on the effective temperature expressed through the effective solid angle of surrounding surfaces [9]. Atoms in the center of the vacuum chamber perceive thermal radiation proportionally to the fraction of the effective solid angle. In our case, the smallest influence is caused by the windows of the vacuum chamber, whose transmittance in the infrared range is small (about 1.5%). The Sr OFS vacuum chamber contains 11 windows with thickness 3.3 mm and area 1662 mm<sup>2</sup> and 2 windows with thickness 2.5 mm and area 254 mm<sup>2</sup>, and their solid angle fraction is small (in total it is approximately 9%). The Sr hot atom source is located at a large distance from the cloud of cooled atoms. The fraction of the solid angle of thermal radiation propagating from it to the center of the vacuum chamber is insignificant (about 0.002%). Thus, the dominant source of thermal radiation is the vacuum chamber walls heated by magnetic coils. They affect a large area of the vacuum chamber in close proximity to the atomic cloud. The fraction of the solid angle perceived by atoms from the vacuum chamber surfaces is approximately 91%.

As measurements using thermal sensors have shown, the vacuum chamber temperature is distributed almost uniformly and averages 23°C. For more accurate knowledge of the vacuum chamber temperature and calculation of the black-body radiation (BBR) shift and its RSE, it is planned to place 10 sensors inside and outside the spectroscope vacuum chamber in the future, but the available data is sufficient for a preliminary estimation of the BBR-induced shift.

To calculate the BBR shift in OFS, the vacuum chamber temperature  $T_{vac}$  is recorded at a distance of about 70 mm from the ultracold atomic cloud. The average temperature of the vacuum chamber during measurements was 292.2 K. Knowing the average temperature, it is possible to calculate the shift caused by BBR using the formula given in [10] and using the values of dynamic and static polarizabilities from [10–13]. Thus, the equation for calculating the BBR (black body radiation, shift) takes the form

$$v_{BBR} = -2.13023(6) \text{Hz} \left(\frac{T}{300 \text{K}}\right)^4 -$$

$$-0.14877(7) \text{Hz} \left(\frac{T}{300 \text{K}}\right)^6.$$
 (1)

Based on the obtained data about the vacuum chamber temperature, the average temperature value  $T_{vac}=292.2\,$  K is calculated. The main sources of uncertainty in estimating the BBR shift are temperature fluctuations of the vacuum chamber from cycle to cycle and the lack of precise information about infrared radiation propagating through the vacuum chamber windows. To calculate the RSE, the vacuum chamber temperature was recorded every 2 hours during one working day. Based on the temperature measurement data, type A uncertainty related to random changes in experimental conditions was calculated

$$u_{A,BBR} = \sqrt{\frac{\sum_{i=1}^{N} (T_i - \overline{T_{vac}})}{N(N-1)}},$$
 (2)

where  $T_i$  is the *i*th temperature measurement,  $T_{vac}$  is the average temperature value, and N is the number of measurements. Type B uncertainty is calculated using the formula

$$u_{B,BBR} = \frac{\Delta_s}{\sqrt{3}},\tag{3}$$

where  $\Delta_s$  — is the measurement error of the TH-485 temperature sensor, which is no more than 0.1 °C in the measurement range from -200 to 60 °C.

The total standard uncertainty of frequency shift measurements caused by BBR is calculated using the formula

$$u_{C,BBR} = \sqrt{u_{A,BBR}^2 + u_{B,BBR}^2}. (4)$$

The expanded uncertainty of measurements with the coverage factor k = 2 was calculated using the formula

$$U_{BBR} = k u_{C,BBR}. (5)$$

Type A uncertainty was  $\pm 0.282$  K, type B uncertainty related to the temperature sensor error was  $\pm 0.057$  K. The uncertainty of indirect measurements for the frequency shift caused by BBR was determined using the formula

$$\sigma_{BBR} = \sqrt{\left(\frac{\delta v_{BBR}}{\delta \overline{T_{vac}}}\right)^2 U_{BBR}^2} =$$

$$(1) = \sqrt{-2.1302 \cdot 4 \frac{\overline{T_{vac}}^3}{300^4} - 0.1487 \cdot 6 \frac{\overline{T_{vac}}^5}{300^6}}.$$
(6)

Thus, the relative uncertainty of the frequency shift estimation caused by BBR is  $2.03 \cdot 10^{-17}$ .

## 2.2. Evaluation of the systematic frequency shift uncertainty component due to the quadratic Zeeman effect

The Zeeman shift in Sr atoms occurs due to the interaction of atoms with an external magnetic field, which causes a shift between the ground and excited states and leads to a shift in the "clock" transition frequency. The first-order Zeeman shift depends on the magnetic quantum number  $m_F$  and the magnitude of the magnetic field B; however, in Sr OFS with precise magnetic field control and the use of repumping lasers, the first-order Zeeman shift can be eliminated, and only the second-order Zeeman shift proportional to  $B^2$  will affect the atoms in the optical lattice

$$\Delta v_Z = \beta \mid B \mid^2 \tag{7}$$

where  $\beta$  is the Zeeman shift coefficient theoretically calculated in [14] and equals  $\beta = -0.233 \text{ Hz/G}^2$ .

Thus, to determine the magnitude of the Zeeman shift in OFS based on ultracold Sr atoms, it is necessary to know the magnetic field value at the location of interaction with atoms (i.e., at the center of the vacuum chamber), applied to split the level  ${}^{3}P_{0}$  into sublevels  $\pm 9/2$ .

When scanning the "clock" transition for sublevels  $\pm 9/2$  the difference between the frequencies of these sublevels is related to the applied constant magnetic field by the following expression [15]

$$\Delta v_{\pm 9/2} = \frac{9\Delta_g \mu_B B}{h} \Rightarrow B = \frac{\Delta v_{\pm 9/2} h}{9\Delta_g \mu_B}, \quad (8)$$

where  $\mu_B$  — is the Bohr magneton, h — Planck's constant, and  $\Delta g = 2.77(3) \cdot 10^{-5}$  — is the differential g-factor between the states  $^3P_0$  and  $^1S_0$  [16].

To evaluate the Zeeman shift, the "clock" transition is scanned and the average frequency difference between sublevels +9/2 and -9/2 is calculated. Then, the magnetic field B is calculated using formula (8). It was determined that the average frequency difference between sublevels +9/2 and -9/2 in the Sr OFS was 1002.3 Hz. This indicates that during spectral analysis, a small magnetic field of B = 1.02 G is applied.

Type A uncertainty associated with magnetic field fluctuations during spectral studies was calculated by fixing the difference value between sublevels +9/2 and -9/2

$$U_{A,\pm 9/2} = \sqrt{\frac{\sum_{i=1}^{N} (\Delta v_{\pm 9/2,i} - \overline{\Delta v_{\pm 9/2,i}})^2}{N(N-1)}}, \quad (9)$$

where  $\Delta v_{\pm 9/2,i}$  is the *i*-th measurement of the frequency difference between sublevels  $\pm 9/2$ ,  $\Delta v_{\pm 9/2,i}$  is the mean value of this frequency difference. Type B uncertainty is calculated using the formula

$$U_{B,\pm 9/2} = \frac{\Delta_{fc}}{\sqrt{3}},$$
 (10)

where  $\Delta_{fc}$  is the frequency meter error, which equals  $2\cdot 10^{-7}$ . The combined standard uncertainty and expanded uncertainty  $U_{\pm 9/2}$  were calculated similarly to the uncertainties for the BBR-induced shift. The uncertainty  $\sigma_B$  of indirect measurements of the magnetic field B was determined using the formula

$$\sigma_B = \sqrt{\left(\frac{\delta B}{\delta v_{\pm 9/2}}\right)^2 U_{\pm 9/2}^2} = \sqrt{\left(\frac{h}{9\Delta_g \mu_B}\right)^2 U_{\pm 9/2}^2}. (11)$$

Then, the uncertainty  $\sigma_Z$  of indirect measurements of the frequency shift caused by the Zeeman effect equals

$$\sigma_Z = \sqrt{\left(\frac{\delta \Delta v_z}{\delta B}\right)^2 \sigma_B^2} = \sqrt{(2\beta B)^2 \sigma_B^2}.$$
 (12)

The conducted evaluations showed that type A uncertainty was  $\pm 2.807$  Hz, and type B uncertainty caused by the frequency meter error was  $\pm 0.000116$  Hz. Thus, the relative standard uncertainty of determining the Zeeman shift was  $\pm 3.18 \cdot 10^{-18}$ .

## 2.3. Evaluation of the OFS component of the dynamic Stark frequency shift

The resonant frequency shift of the "clock" transition in the optical lattice is associated with the dynamic Stark shift arising from the presence of the confining optical potential. The optical lattice is a

standing wave formed by two laser beams (direct and reflected), in whose potential wells the cooled atoms are loaded. The standing wave is created by a high-power laser. The laser beam is focused using a lens to achieve the minimum possible waist radius (the narrowest point of the focused laser beam) in the interaction region of the OLFL radiation with cooled atoms and is reflected by a mirror in the opposite direction without changing the radiation polarization.

In OFS Sr-1, OLFL is stabilized using an Angstrom WS U2 wavemeter, with a calibration error of  $\pm 2$  MHz. In order to keep atoms in the potential wells of the standing wave, the potential well depth of the optical lattice must be greater than the thermal motion energy of atoms cooled in magneto-optical traps (MOT). Using the expression for the potential well depth of a one-dimensional optical lattice [16] and expressing it through the frequency  $v_z$  of the longitudinal sideband, we obtain

$$U = \frac{\mathbf{v}_z M^2 \lambda^4}{h^2} E_r,\tag{13}$$

where M — is the atom mass,  $\lambda$  — is the radiation wavelength, and  $E_r = 3.47 \text{ kHz}$  — is the photon recoil energy [17].

To determine the value  $v_z$ , it is necessary to conduct spectral studies using the "clock" laser in a wide range and determine the frequency value of the sideband caused by atomic oscillations in the optical lattice. Knowing the frequency  $v_z$ , one can determine the depth U of the holding potential of the potential well of the optical lattice standing wave by formula (13).

In [17], it was shown that the depth of the optical lattice trapping potential can also be calculated within the dipole approximation through the polarizabilities of the "clock" levels and radiation intensity

$$U = \frac{\alpha_{e(g)}(\omega_m)I}{E_r},\tag{14}$$

where  $\alpha_e$  and  $\alpha_g$  are the electric dipole dynamic polarizabilities of the ground and excited states, respectively, and I is the OLFL radiation intensity at the point of interaction with atoms. At the "magic" wavelength ("magic" frequency  $\omega_m$ ), the polarizability of Sr atom equals 241.3 at. units or 42.2 kHz/(kW·cm<sup>-2</sup>) [18]. The radiation intensity is determined by the formula

$$I = \frac{2P}{\pi w_0^2},\tag{15}$$

where P is the radiation power and,  $w_0$  is the laser beam waist diameter at the point of interaction with atoms. Therefore, by measuring the OLFL radiation power and calculating the depth of the optical lattice trapping potential using formulas (13)–(15), one can calculate the waist diameter

$$w_0 = \sqrt{\frac{2P\alpha_{e(g)}(\omega_m)}{\pi U E_r}}. (16)$$

Knowing the OLFL laser beam waist diameter, it is easy to calculate its intensity using formulas (15), (16). The frequency shift caused by the OLFL radiation spectrum can be calculated using the integral by the formula [18]

$$v_L = -\int_0^\infty \Delta\alpha(\omega) I(\omega) d(\omega), \qquad (17)$$

where  $\Delta\alpha(\omega) = \alpha_e(\omega) - \alpha_g(\omega)$ ,  $I(\omega)$  is the spectral distribution of OLFL radiation intensity. Since the amplified spontaneous emission spectrum was filtered using a single-mode optical fiber, the OLFL radiation spectrum represents a narrow spectral line. The uncertainty in measuring the OLFL shift can be estimated as the product of OLFL radiation intensity and the difference of electric dipole dynamic polarizabilities at the maximum deviation of OLFL radiation from the magic wavelength. In our case, the maximum deviation from the magic wavelength equals the wavemeter error.

Dynamic polarizabilities were determined in [17]. Near the magic wavelength, their difference changes linearly, which allows using the slope coefficient of the line to calculate the shift caused by OLFL.

The wavemeter calibration error leads to the value of dynamic polarizabilities difference at the maximum deviation from the magic wavelength being  $\pm 2.242 \cdot 10^{-6}$  at. units or  $\pm 4.205 \cdot 10^{-7}$  kHz/(kW·cm<sup>-2</sup>).

The standard type A uncertainty caused by random fluctuations of the measurement of  $v_z$  was calculated. It was 0.4 kHz. Type B uncertainty is also related to the frequency meter error and equals  $6 \cdot 10^{-6}$  kHz.

The influence of uncertainty in radiation power *P* measurement was also taken into account. The

standard type A uncertainty of radiation power P measurement was  $u_{AP} = 0.34$  mW, type B uncertainty associated with the power meter error  $(\pm 0.5\%)$  is  $u_{BP} = 2$  mW. Then, the expanded standard uncertainty of power measurement equals

$$U_P = K \sqrt{u_{AP}^2 + u_{BP}^2}. (18)$$

For calculating the radiation intensity uncertainty in indirect measurements, the following formula was used

$$\sigma_{I} = \sqrt{\left(\frac{\partial I}{\partial \omega_{0}}\right)^{2} \sigma_{\omega}^{2} + \left(\frac{\partial I}{\partial \overline{P}}\right)^{2} U_{P}^{2}} =$$

$$= \sqrt{\left(-\frac{4P}{\pi \omega_{0}^{3}}\right)^{2} \sigma_{\omega}^{2} + \left(\frac{2}{\pi \omega_{0}^{2}}\right)^{2} U_{P}^{2}}, \quad (19)$$

where  $\sigma_{\omega}$  is the uncertainty of radiation waist calculation, which was less than several units  $10^{-18}$ . Then, the uncertainty of frequency shift caused by OLFL equals

$$\sigma_L = \Delta \alpha(\omega) I \sigma_I [Hz].$$
 (20)

Thus, the OLFL calibration error with respect to the wavemeter, as well as variations in OLFL radiation power lead to a relative uncertainty in measuring the frequency shift caused by OLFL radiation with intensity of  $14 \text{ kW/cm}^2$  at a waist of  $90 \mu \text{m}$ , at the level of  $1.4 \cdot 10^{-17}$ .

## 2.4. Total systematic uncertainty of Sr-1 optical frequency standard

The total measurement uncertainty of Sr-1 OFS according to our latest estimates is at the level of  $2.5 \cdot 10^{-17}$ . The main contributions to RSE are given in Table 1.

Table 1. RSE budget of Sr-1 OFS

Frequency shift	RSE, $1 \cdot 10^{-17}$	
Zeeman shift	0.3	
OLFL shift	11.4	
BBR shift	2.5	

#### 3. DESIGN OF TRANSPORTABLE OFS

Currently, transportable hydrogen masers [19] are used to compare geographically remote standards, with their frequency instability not exceeding several units of  $10^{-16}$  per day.

The next step in improving the characteristics of mobile complexes will be to equip them with optical standards. For example, placing a highly stable laser with a wavelength of 1.5 µm and a femtosecond optical frequency synthesizer in a mobile complex will improve the short-term stability of the complex. This will also allow, given the available fiber-optic communication line (FOCL) channel, to transmit a signal at optical frequency over long distances. This will increase the speed of hydrogen maser frequency calibration against a remote stationary OFS.

The development of full-fledged mobile or relocatable OFS is a relevant task that many laboratories worldwide are working on. The solution to this task is outlined in the "roadmap". We are developing relocatable OFS based on ultracold atoms  $^{171}\mathrm{Yb}$ . Figure 1 shows its possible implementation in a van. The van size for housing the transportable OFS is  $7500\times2550\times2100~\mathrm{mm}^3$ . It consists of three compartments, viz. operator compartment, physical part with optical spectroscope, frequency formation and distribution scheme, and other equipment; frequency measurement compartment.

The physical part for relocatable OFS using ytterbium atoms was completely redesigned compared to the stationary OFS design using strontium atoms. A modular design was chosen as the foundation. The heart of the relocatable OFS system is a compact optical spectroscope module with a vacuum chamber, a hot atom source, and a detection system. Laser radiation is delivered to the spectroscope through single-mode polarizationmaintaining optical fibers from the laser systems module. Radiation at wavelengths of 399 and 556 nm passes through the frequency distribution scheme to form the necessary frequency detunings for the Zeeman slower, MOT, and detection. The frequencies of all laser systems are stabilized using the Pound-Drever-Hall method through a compact module based on high-Q optical resonators.

The resonator body is made of material with a low expansion coefficient. The total size of the frequency stabilization module does not exceed 250 mm in the sum of three dimensions.

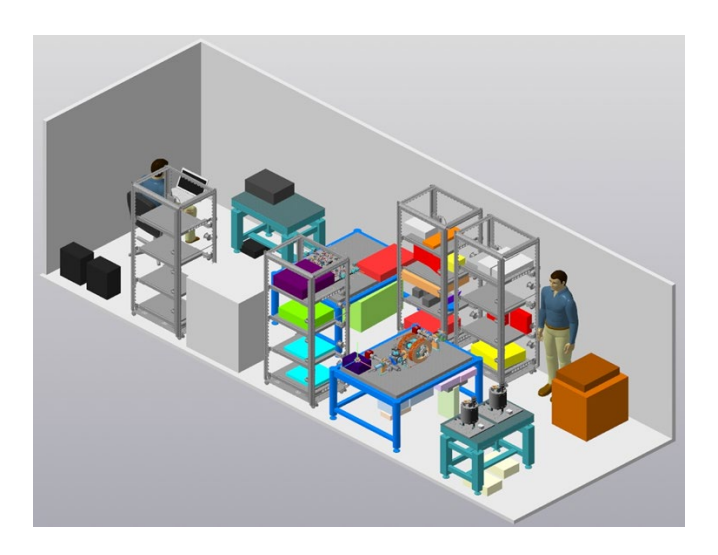


Fig. 1. Designed arrangement of OFS components in a van. The van is divided into three compartments, viz. operator compartment, OFS physical part compartment, and frequency measurement compartment. The operator compartment contains a personal computer with a control system and uninterruptible power supplies. The OFS physical part compartment houses the optical spectroscope, radiation distribution scheme, and auxiliary equipment. The last compartment contains highly stable laser systems and femtosecond optical frequency synthesizer.

The transportable OFS based on ytterbium atoms consists of a spectroscope with a vacuum level not worse than  $5 \cdot 10^{-9}$  mBar maintained by getter-ion pumps. The spectroscope size is  $50 \cdot 130$  cm<sup>2</sup>. The BBR influence due to heating of magnetic coils forming MOT is optimized using the finite element method. The coils generate a magnetic field with a gradient of 25 G/cm, and their maximum temperature is  $50^{\circ}$ C. Several temperature sensors located in the chamber housing allow for more accurate determination of the RSE of the unperturbed "clock" transition frequency shift in ytterbium atoms due to BBR.

The laser source module uses diode and fiber laser systems for all required wavelengths, except for the "clock" transition wavelength 399 nm (primary MOT, detection, and Zeeman beam), 556 nm (secondary MOT), 759 nm (optical lattice), 1388 nm (repumping laser). To form frequency detuning and switch laser radiation on/off at the required instants of OFS operation cycles, a radiation distribution scheme at wavelengths of 399 and 556 nm is used. The necessary frequency detunings are formed using acousto-optical modulators (AOM) designed at VNIIFTRI [20]. AOMs together with mechanical shutters also participate in switching laser radiation on/off. The size of this module is  $600 \cdot 00 \text{ mm}^2$ .

The laser radiation frequency stabilization module consists of two Fabry-Perot resonators made of a solid piece of material, with finesse more than 20,000 for IR wavelengths. The resonators are kept in vacuum and temperature-controlled. Tests show that when the frequency stabilization module deviates from vertical by an angle up to  $20^{\circ}$ , the laser frequency shift does not exceed 100 kHz.

In a separate compartment, there are laser systems with ultra-narrow emission spectral linewidth, viz. a "clock" laser and a laser with a 1.5 µm emission wavelength. The "clock" laser system is based on a diode laser with an external resonator, which is located in a single housing with a high-Q resonator. It generates radiation at a wavelength of 1156 nm, which is convenient for high-Q mirror coating and optical frequency transfer up to 1 km (see Section 4.3). To probe the "clock" transition in ultracold ytterbium atoms, a wavelength of 578 nm is required, which is generated using a frequency-doubling crystal based on a PPLN waveguide structure.

This compartment also houses a 1.5  $\mu m$  wavelength laser, which is necessary for rapid comparisons of OFSs separated by distances of more than 1 km, with accuracy better than several units of the 17th digit.

The transportable OFS is controlled using a compact control system [21], which consists of a personal computer with control software installed and hardware based on an STM32 microcontroller and plug-in modules. The microcontroller board

size is  $11 \cdot 26 \text{ cm}^2$ , which allows it to fit in the limited space of the van.

Overall, the mass and dimensional parameters of the transportable OFS are 2–3 times smaller than those of the stationary OFS based on ultracold Sr atoms, and the system's power consumption is reduced by 2 times. The predicted RSE of the OFS is less than  $1 \cdot 10^{-17}$ , which is possible due to precise temperature control inside the spectroscope and precision stabilization of the laser frequency forming the optical lattice.

### 4. USING FIBER-OPTIC COMMUNICATION LINES FOR COMPARING FREQUENCIES OF REMOTE FREQUENCY STANDARDS

# 4.1. Principle of transmitting highly stable frequency signals of microwave and optical standards via fiber-optic communication lines

Geographically remote standards, both microwave and optical, can be compared by frequency using fiber-optic communication lines to deliver the output signal from one standard to another. To transmit radio frequency output signals of microwave standards, amplitude modulation of the laser carrier propagating in the fiber line is used. There are no high requirements for the laser carrier characteristics. Most commonly, distributed feedback semiconductor lasers are used for these purposes, with wavelengths corresponding to the optical fiber transparency windows of 1.55 and 1.31 µm. Without intermediate optical amplifiers in the fiber line, a highly stable radio frequency output signal of a microwave standard can be transmitted on a 1.55 µm optical carrier through a compensated fiber line for distances up to 100 km. To date, transmission systems have been created worldwide and experiments have been conducted to transmit reference frequency and time signals through dedicated fiber lines for distances up to 500 km. To compensate for optical carrier attenuation in such lines, intermediate optical amplifiers EDFA (erbium doped fiber amplifier) are installed every 60 - 80km [22].

The output radiation of the "clock" laser of an optical standard carrying information about its frequency can be directly transmitted through a fiber line. However, the frequency of practically all highly stable optical standards does not correspond

to fiber transparency windows. Therefore, without frequency conversion of the optical standard "clock" laser to the fiber transparency window range, its radiation is transmitted only in relatively short fiber lines. For long-distance transmission, preliminary conversion of the optical frequency standard "clock" laser radiation to the main fiber transparency window range of 1.55 µm is necessary. Femtosecond optical frequency synthesizers are used for such conversion. Without intermediate optical amplifiers in the fiber line, highly stable optical radiation at 1.55 µm wavelength can be transmitted through a compensated fiber line for distances up to 80 km.

Note that optical fiber is a material medium that disturbs the highly stable signal propagating through it. Furthermore, the physical properties of the fiber are sensitive to environmental factors at the fiber line installation locations. Therefore, the optical signal transmitted through the fiber line accumulates phase disturbances as it propagates along the line. This leads to loss of its frequency stability and Doppler shifts due to drift in the optical length of the line caused by variations in ambient temperature. The radio frequency output signal of the best microwave standards can be transmitted via a fiber line without loss of accuracy for distances up to a kilometer. However, the radiation from optical standards, which have characteristics two orders of magnitude higher compared to microwave standards, begins to lose its high stability at fiber line lengths of several meters.

To date, various systems for transmitting highly stable optical and radio frequency signals have been developed and experimentally tested, ensuring compensation for signal phase disturbances introduced by the fiber line [23, 24]. All such systems use the method of signal propagation along the line in forward and reverse directions and subsequent comparison of the phases of the returned and original signal fed to the line input. Based on such comparison, an error signal is generated, which is used to correct the phase of the transmitted highly stable signal before sending it through the fiber line. Such preliminary phase correction of the transmitted signal provides compensation for disturbances, viz. additional phase noise introduced by the fiber line. When transmitting a radio frequency signal of a microwave standard, its phase correction can be performed, for example, using controlled electronic or optical delay lines. The contribution of the compensated fiber system to the error of the

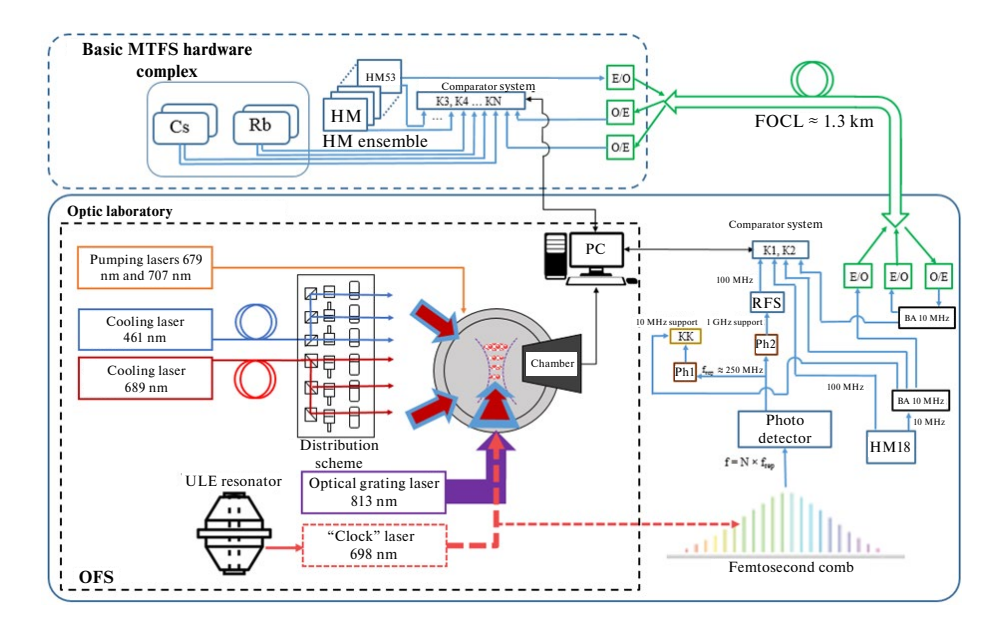


Fig. 2. Scheme of Sr-1 OFC composition, master time and frequency standard hardware complex and OFC frequency transmission and comparison system and microwave standards. BA stands buffer amplifier, Ph1 and Ph2 stand for photodetectors, KK stands for K+K frequency counter, RFS stands for radio frequency synthesizer, K1, K2, K3,...,KN stand for comparators, E/O stands for electro-optical converter, O/E stands for optoelectrical converter, Cs stands for frequency references based on cesium fountain, Rb stands for frequency standards based on rubidium fountain, and HM stands for hydrogen masers.

transmitted radio frequency signal value lies at the level of  $10^{-17}$  with the averaging time  $10^5$  s [24].

When transmitting OFS optical radiation, an AOM is used as a correction device in the compensation system. The phase-correcting AOM is connected in series at the beginning of the fiber line according to the scheme proposed and first implemented in [25]. The error signal supplied to the AOM controls the phase of the transmitted highly stable optical radiation, compensating for phase noise introduced by the fiber line. Using this scheme, experiments have been performed worldwide to transmit radiation from highly stable lasers with a wavelength of 1.55 µm through dedicated compensated fiber lines over distances up to 2000 km [26]. The system's contribution to the optical frequency transmission error was below  $10^{-18}$  at an averaging interval of 10<sup>5</sup> s. To compensate for optical radiation attenuation in such long lines, intermediate optical EDFA or Brillouin amplifiers were used [26,27].

# 4.2. System for transmission and frequency comparison via fiber-optic lines of microwave and optical standards included in GET-1

To compare the OFS frequency on ultracold atoms Sr-1 and hydrogen masers from GET-1, the

10 MHz output signals from hydrogen masers are transmitted through fiber-optic lines. These 1.3 km lines connect the main hardware complex of the State Primary Time and Frequency Standard and the remote optical laboratory where the OFS is located. A simplified diagram of the OFS composition, the State Primary Time and Frequency Standard hardware complex, and the radio frequency signal transmission system is shown in Fig. 2.

In the optical laboratory, an HM18 hydrogen maser with a frequency of 100 MHz is installed, which is compared with OFS Sr-1 using a femtosecond optical frequency synthesizer and comparator K1 (HF-315). The frequency of the HM18 maser is also compared using comparator K2 with the transmitted 10 MHz signal from the hydrogen maser HM53. In turn, the 10 MHz signal from the HM18 maser is transmitted to the main hardware complex of MTFS, where it can be frequency-compared by comparators K3-KN with an ensemble of hydrogen masers, as well as with standards based on rubidium and cesium fountains.

Research results showed that the random error in measuring the frequency of OFS on Sr atoms with an ensemble of hydrogen masers is determined by the inherent noise of hydrogen masers, and the communication line itself does not introduce significant error in measurement results [28].

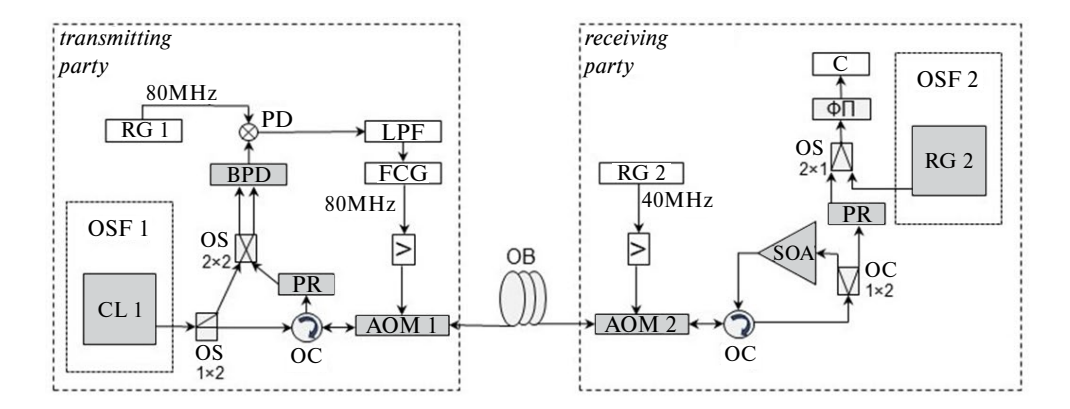


Fig. 3. Scheme of the system for transmitting radiation from the "clock" laser CL 1 at 1156 nm through a compensated fiber-optic line FO and comparing frequencies of "clock" lasers CL 1 and CL 2 of remote OFS 1 and OFS 2 on ytterbium atoms. OS stands for optical splitters, OC stands for optical circulators, PR stands for polarization rotators, PD stands for phase detector, LPF stands for low-pass filter, FCG stands for frequency-controlled generator, AOM 1 and AOM 2 stand for acousto-optic bidirectional modulators at 80 MHz and -40 MHz, RG 1 and RG 2 stand for radio generators, BPD and PD stand for balanced photodetector and photodetector, SOA stands for semiconductor optical amplifier, and M stands for electronic frequency meter

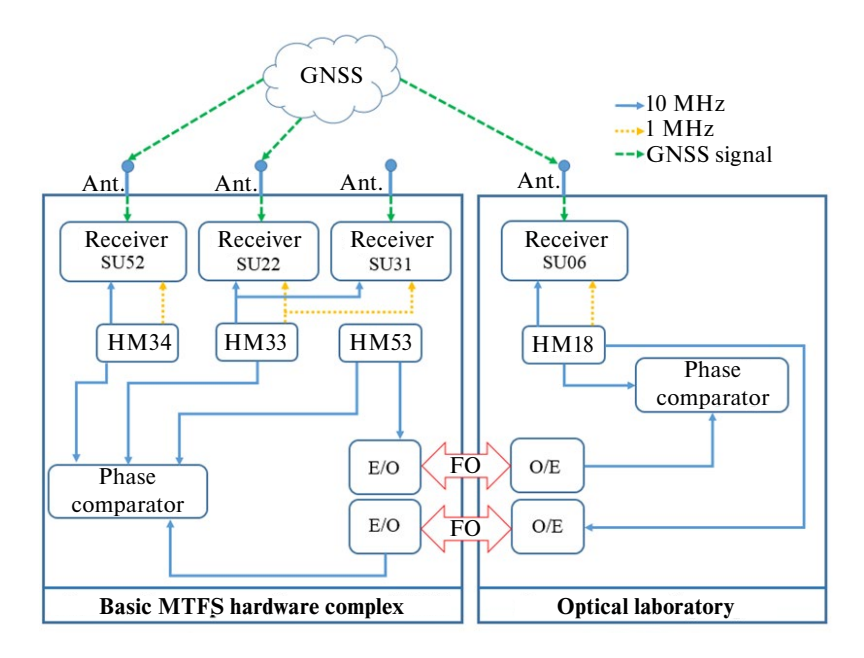
# 4.3. System for fiber-optic transmission and frequency comparison of relocatable optical standards based on ytterbium atoms

Figure 3 shows the scheme of the system for transmitting radiation through a fiber-optic line (FO) from a highly stable "clock" laser CL 1 at a wavelength of 1156 nm. It is constructed on the basis of a fiber interferometer that ensures compensation for accumulated phase noise in the FO. This system was developed by us to compare frequencies of two relocatable optical standards based on ytterbium atoms, OFS 1 and OFS 2, which can be separated by several kilometers.

The design of transportable OFS must be compact and ensure the possibility of transporting the standard on the Earth's surface, as well as simple assembly and conversion to the operational state. The transportability feature of OFS allows such a standard to be used as a reference for frequency comparison between stationary OFS located at a distance from each other. Additionally, a pair of transportable OFS connected by a compensated fiber line can provide measurements of gravitational potential differences between points on Earth where the standards are installed. The need for such measurements is related to the fact that quantum standards' frequency is affected by the relativistic shift. Therefore, one of the requirements of the "roadmap" for transitioning to a new definition of the second lies in more precise knowledge of the geopotential at OFS locations. This can be achieved

by combining regional geodetic information with a global model and supplementing it with results from OFS frequency comparisons at different points on Earth. Note that for geopotential modeling, satellite data provides reliable information only at spatial resolutions of 200 km or worse. Currently, individual metrology laboratories estimate gravitational shifts of OFS with uncertainty at the level of  $10^{-18}$  [4].

The concept of noise compensation in the fiber transmission system shown in Fig. 3 is similar to that proposed in [25], yet it has some peculiarities. They are associated with the fact that the scheme has no optical elements operating in the free space. The transmission of radiation from the "clock" laser CL 1 is carried out without conversion to the transparency range of optical fiber at 1.55 µm. The transmission is performed directly at a wavelength of 1156 nm This significantly increases the system reliability and simplifies the frequency comparison of CL 1 and CL 2. This system does not use complex femtosecond optical frequency synthesizers However, note that at 1156 nm wavelength, both the optical fiber and all fiber-optic elements in the system, such as optical circulators, splitters, and AOM have significantly higher losses than similar elements designed to operate at 1.55 µm wavelength. In the scheme shown in Fig. 3, at 1156 nm wavelength, the optical loss budget with a 5 km fiber line reaches 26 dB. Note that such a loss budget corresponds to losses in a system transmitting laser radiation at 1.55 um wavelength through a 100 km fiber line.



**Fig. 4.** Experimental setup for determining the frequency comparison error of remote frequency standards using GNSS. HM stands for reference active hydrogen frequency standards, E/O stands for electro-optical converter, O/E stands for optical-electrical converter, and Ant. stands for GNSS receiver antenna

We also emphasize that the working quantum transition in the Yb atom has a wavelength of 578 nm. However, we chose a laser with a wavelength of 1156 nm, and radiation at 578 nm wavelength for spectral analysis of the "clock" transition is formed using a doubling crystal. The choice of a longer wavelength "clock" laser at 1156 nm facilitates the task of transmitting radiation through fiber lines over long distances. This is because a long fiber-optic line would have very high losses in the shorter wavelength region of 578 nm.

Optical circulators OC in the system (Fig. 3) ensure separation of radiation propagating in the fiber line in forward and backward directions. The balanced photodetector BPD mixes the initial radiation fed into the line with the radiation returned from the receiving side. The error signal required for phase correction is generated at the phase detector PD after comparing the frequency of optical beats obtained at the BPD with the reference generator RG 1 at 80 MHz. Compensatory phase correction of optical radiation in the line is implemented by acousto-optic modulator AOM 1.

The radiation received at the receiving side through the optical fiber FO is fed to a bidirectional acousto-optic modulator AOM 2 at a frequency of -40 MHz (see Fig. 3). This AOM 2 is controlled by a stable 40 MHz radio signal. The 40 MHz

shifted optical radiation passing through the optical circulator OC is divided by an optical splitter OS into two directions. One part of the radiation is amplified by a semiconductor optical amplifier SOA and returned back to the beginning of the line at the transmitting side. The second part of the radiation is fed to a photodetector PD, where it is mixed with the radiation from the "clock" laser CL 2 from OFS 2. Measuring the 40 MHz beat frequency isolated at the PD using an electronic frequency counter allows comparing the frequencies of OFS 1 and OFS 2 with high accuracy.

### 5. COMPARING REMOTE OFS FREQUENCIES USING GNSS SIGNALS

On-board microwave standards installed on spacecraft of global navigation satellite systems (GNSS) and their emitted signals can be used as unique reference standards for determining the frequency difference of OFS installed on Earth. Creating systems that use GNSS signals for comparing frequencies of remote OFS is significantly cheaper than fiber-optic systems as it does not require laying expensive communication channels [29]. GNSS receivers are widely available, inexpensive, and require practically no operational costs.

However, an important issue is studying the frequency comparison error of remote OFS achievable when using GNSS signals. A series of experiments was conducted to evaluate this error [30]. The experiment compared the frequencies of three hydrogen masers located at MTFS facilities at a distance of approximately 850 m from each other. The experimental setup is shown in Fig. 4.

The basic MTFS hardware complex (Signal facility) housed three GNSS receivers and two reference active hydrogen frequency standards (HM). The optical laboratory building contained one GNSS receiver and one HM. Another HM in the basic MTFS hardware complex was used as an intermediate for frequency comparison via fiber-optic communication lines (FOCL). During the experiment, frequency difference estimates of reference HMs were obtained using GNSS and two independent FOCL lines. This allowed for comparison of results obtained via GNSS and FOCL. Assuming that the error in HM frequency transmission via FOCL is negligibly small compared to the error arising from using GNSS channels, the error in HM frequency difference estimates via GNSS was determined.

The determination of HM frequency differences using GNSS in the experiment was conducted based on time scale (TS) divergence estimates by forming a simple first difference of TS. To determine the TS difference, a high-precision absolute positioning technique with integer precise point positioning (IPPP or PPP-AR) [31, 32] was used. The input data for this technique includes code and phase measurements from the GNSS receiver in two frequency bands. Information about high-precision orbits and corrections to the onboard TS of navigation satellites is also required. For high-precision TS comparison, it is necessary to accumulate code and phase GNSS measurements over several days. An important condition is the continuity of phase measurements throughout the entire time interval of problem solving.

The advantage of IPPP technology lies in obtaining a unified solution across the entire array of processed measurements under the condition of continuous phase measurements. Such a solution, unlike the traditional high-precision PPP positioning method, is not affected by inter-daily jumps and other factors that degrade accuracy. As a result, the difference in time scale discrepancies

between any instants within the processing interval can be determined with very high accuracy. However, for each processing session, there will be a constant error in the time scale estimation, which depends on code measurement noise and several other factors. However, since the absolute value of the time scale difference is not important for solving the frequency difference measurement task, only the phase difference of time scales needs to be known. Thus, the constant error of the time scale difference does not affect the result, and the error in frequency difference estimation is determined only by the random component of phase measurements and the models used in the solution. The random error of time scale estimation using the IPPP method is estimated as not exceeding 50 ps, which corresponds to a frequency comparison error of the order of  $\pm 1 \cdot 10^{-16}$  per day. Another important advantage of IPPP technology is that simultaneous visibility of satellites is not required. Of course, within this experiment, this is not crucial since the receivers were located only 850 m apart, but when performing comparisons at distances of several thousand kilometers, this factor becomes of primary importance.

The experiment was conducted over four months: from September 29, 2022 to January 29, 2023. This allowed evaluating the stability of IPPP solutions for intervals up to two months. The modified Allan deviation, which is commonly used to evaluate comparison channel characteristics, was chosen as the measure of error in the experiment. First, the difference between frequency estimates obtained from measurements using different GNSS receivers (IPPP) and measurements via fiber optic links using a phase comparator was calculated. Then, the deviations of these differences were calculated, which are shown in Fig. 5. The *y*-axis shows the modified Allan deviation directly, while the *x*-axis shows the averaging time in days.

As can be seen from the presented graph, with averaging from 20 days, the IPPP method makes it possible to compare frequencies of remote standards with an uncertainty of several unit  $10^{-17}$  provided that phase measurements are continuous and there are no processing problems. The dashed line on the graph shows the modified Allan deviation of the theoretical noise process with phase flicker noise of 35 ps. For such a process, this value decreases linearly with increasing averaging time. The

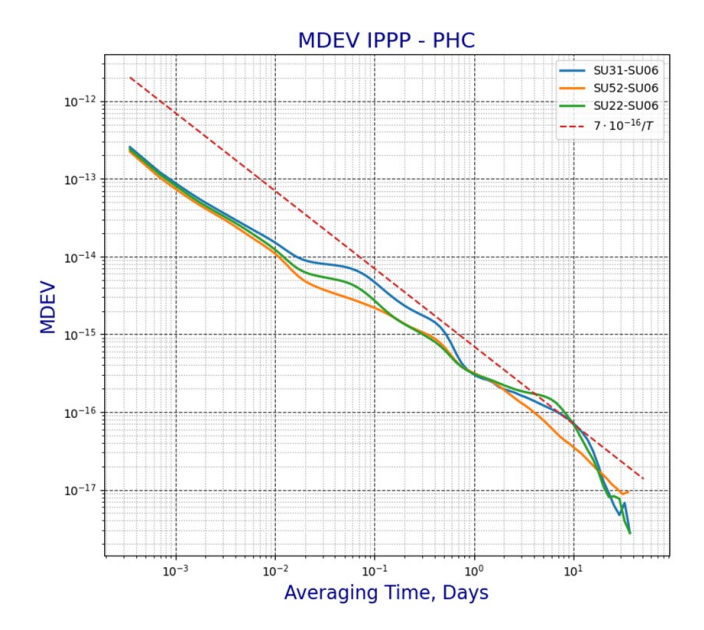


**Fig. 5.** Modified Allan Deviation (MDEV) of frequency difference determination error using IPPP (PHC stands for the phase comparator)

proximity of the obtained results to this process at large averaging intervals suggests a further tendency of the IPPP method error reduction also according to a linear law depending on the averaging time.

Foreign specialists also conducted experiments comparing estimates obtained by IPPP method and through optical frequency comparison channel. In the foreign experiment, a significantly longer FOCL line was used and it was shown [33] that the random error of the IPPP method also did not exceed  $1 \cdot 10^{-16}$  for averaging interval of 3 days for baselines up to 1000 km. This corresponds to the results obtained during our experiment. Conducting comparisons on longer baselines to verify the method is difficult due to the lack of an alternative fiber-optic or any other channel for transmitting highly stable signals with the required accuracy.

A disadvantage of using the IPPP method for comparing frequencies of remote OFS is the need for long-term averaging to achieve the required accuracy. This limits the method's application and does not allow for direct comparison of OSF frequencies since the continuous operation time of OFS typically does not exceed several days. Therefore, it is necessary to use microwave HM as intermediate clocks, which are compared using IPPP, while OSF, in turn, are compared with HM.

Table 2. Comparing OFS frequency comparison methods

Methods	FOCL	TOSF	GNSS
Achieva- ble RSE	< 5 · 10 <sup>-19</sup>	$< 3 \cdot 10^{-17}$	$\sim 5\cdot 10^{-17}$
Advan- tages	High accuracy due to compensation of phase noise introduced by FOLC	Flexibility since transportable OSF can be moved to any point	Widely used, less expensive
Disad- vantages	In Russia, it is hard to use telecommunication FOCL to transmit high stability signal	It is technically difficult to achieve metrological characteristics, at the level of stationary OSF	Long averaging is required (> 20 days)

#### 6. CONCLUSIONS

In this work, we refine the uncertainty budget components of the OFS Sr-1, which is part of GET-1. This allowed estimating its total systematic uncertainty budget at the level of  $2.5 \cdot 10^{-17}$ . The intra-facility system for frequency transfer and comparison via fiber-optic communication lines for microwave and optical standards included in GET-1 is described.

A preliminary design of a relocatable OFS using ultracold neutral ytterbium atoms is presented, and a scheme for comparing optical frequencies of spatially separated relocatable ytterbium-based OFS via fiber-optic links is described.

An experimental comparison of methods for comparing output signals of microwave frequency standards using fiber-optic links and GNSS signals was conducted. For this purpose, measurements were performed to compare the results of frequency comparisons of geographically distributed hydrogen masers within GET-1 obtained through fiber-optic signal transmission and the IPPP method.

The comparison of three considered methods for frequency comparison of two remote OFS is shown above in Table 2.

Each method has its advantages and disadvantages, but the GNSS signal comparison method appears to be the most achievable at present due to its relative ease of use, although it requires data averaging over 20 days. In conclusion, we note that adopting a new definition of the second requires the ability to compare OFS frequencies on continental and transcontinental scales. It is expected that future optical standard frequency comparisons will be based on signal transmission in local fiber-optic networks connected by non-fiber intercontinental communication lines [29]. Therefore, it is necessary to develop all three OFS comparison methods indicated in Table 2.

#### **REFERENCES**

- 1. J. Terrien, Metrologia 4, 41 (1968).
- 2. G. Petit, F. Arias, and G. Panfilo, Compt. Rend. Phys. **16**, 480 (2015).
- 3. T. Bothwell, D. Kedar, E. Oelker et al., Metrologia **56**, 65004 (2019).
- **4.** N. Dimarcq, M. Gertsvolf, G. Mileti et al., Metrologia **61**, 012001 (2024).
- S. I. Donchenko, I. Yu. Blinov, I. B. Norets et al., Meas. Tech. 1, 35 (2020).
- **6**. D. V. Sutyrin, O. I. Berdasov, S. Yu. Antropov et al., Ouantum Electron. **49**, 199 (2019).
- 7. G. S. Belotelov, D. V. Sutyrin, S. N. Slyusarev, Almanac of Modern Metrology **4**, 100 (2021).
- **8**. A. P. Vyalykh, P. I. Skakunenko, M. V. Shishova et al., Letters to JETP **119**, 273 (2024).
- D. Xiong, Q. Zhu, J. Wang et al., Metrologia 58, 35005 (2021).
- **10**. T. Middelmann, S. Falke, C. Lisdat et al., Phys. Rev. Lett. **109**, 263004 (2012).
- **11**. S. G. Porsev and A. Derevianko, Phys. Rev. A **74**, 20502 (2006).
- **12**. M. S. Safronova, S. G. Porsev, U. I. Safronova et al., Phys. Rev. A **87**, 12509 (2013).
- **13**. T. L. Nicholson, S. L. Campbell, R. B. Hutson et al., Nat. Commun. **6**, 6896 (2015).
- **14**. A. V. Taichenachev, V. I. Yudin, C. W. Oates et al., Phys. Rev. Lett. **96**, 83001 (2006).

- X. Baillard, M. Fouche, R. Le. Targat et al., Eur. Phys. J. D 48, 11 (2008).
- **16**. M. M. Boyd, T. Zelevinsky, A. D. Ludlow et al., Phys. Rev. A **76**, 22510 (2007).
- **17**. V. D. Ovsiannikov, S. I. Marmo, V. G. Palchikov et al., Phys. Rev. A **93**, 43420 (2016).
- **18**. G. S. Belotelov, V. D. Ovsiannikov, D. V. Sutyrin et al., Laser Phys. **30**, 45501 (2020).
- **19**. I. Yu. Blinov, Yu. F. Smirnov, F. R. Smirnov, Vestnik Metrologa **3**, 3 (2018).
- 20. M. M. Mazur, L. I. Mazur, V. N. Shorin et al., Quantum Electronics 52, 661 (2022).
- 21. A. V. Semenko, A. P. Vyalykh, D. A. Paryohin et al., in *Proc. 26th Int. Conf. on Digital Signal Processing and its Applications* (DSPA), IEEE (2024), pp.1-5.
- 22. V. Smotlacha, A. Kuna, and W. Mache, in *Proc. of the 42nd Annual PTTI* (2010), p. 427.
- 23. K. Yu. Khabarova, E. S. Kalganova, N. N. Kolachevsky, Physics-Uspekhi 188, 221 (2018).
- **24**. R. I. Balaev, A. N. Malimon, D. M. Fedorova et al., Measurement Techniques **38** (2017).
- **25**. L.-S. Ma, P. Jungner, J. Ye et al., Opt. Lett. **19**, 1777 (1994).
- **26**. S. Droste, F. Ozimek, Th. Udem et al., Phys. Rev. Lett. **111**, 110801 (2013).
- **27**. O. Terra, G. Grosche, and H. Schnatz, Opt. Express **18**, 16102 (2010).
- 28. D. V. Sutyrin, A. Yu. Gribov, R. I. Balaev et al., Quantum Electronics 52, 498 (2022).
- **29**. M. Pizzocaro, M. Sekido, K. Takefuji et al., Nat. Phys. **17**, 223 (2021).
- **30**. V. F. Fateev, A. A. Karaush, F. R. Smirnov, Technical Physics **93**, 23 (2023).
- **31**. P. Collins, S. Bisnath, F. Lahaye et al., Navigation **57**, 123 (2010).
- **32**. S. Loyer, F. Perosanz, F. Mercier et al., J. Geod. **86**, 991 (2012).
- **33**. G. Petit, J. Leute, S. Loyer, and F. Perosanz, in *Proc. Joint Conf. EFTF/IFCS*, IEEE (2017), p. 784